Preclinical Evaluation and Pilot Clinical Study of Al^{18}F-DX600-BCH for non-invasive PET Mapping of Angiotensin Converting Enzyme 2 in Mammal

Jin Ding
Peking University Cancer Hospital: Beijing Cancer Hospital
Qian Zhang
Peking University Cancer Hospital: Beijing Cancer Hospital
Jinquan Jiang
Peking University Cancer Hospital: Beijing Cancer Hospital
Nina Zhou
Peking University Cancer Hospital: Beijing Cancer Hospital
Zilei Wang
Peking University Cancer Hospital: Beijing Cancer Hospital
Xiangxi Meng
Peking University Cancer Hospital: Beijing Cancer Hospital
Teli Liu
Peking University Cancer Hospital: Beijing Cancer Hospital
Feng Wang
Peking University Cancer Hospital: Beijing Cancer Hospital
Zhihao Lu
Peking University Cancer Hospital: Beijing Cancer Hospital
Xing Yang
Peking University First Hospital
Zhi Yang
Peking University Cancer Hospital: Beijing Cancer Hospital
Hua Zhu (zhuhuaBCH@pku.edu.cn)
Peking University Cancer Hospital: Beijing Cancer Hospital

Research Article

Keywords: ACE2, SARS-CoV-2, DX600, PET

Posted Date: November 29th, 2021

DOI: https://doi.org/10.21203/rs.3.rs-1059130/v1

Abstract

Angiotensin-converting enzyme 2 (ACE2), a transmembrane protein, is the main entry point for certain coronaviruses including the new coronavirus SARS-CoV-2 to enter cells. Synthesizing the PET imaging probe Al^{18}F-DX600-BCH which is high-affinity ACE2 is aim to detect the expression of ACE2 in body and monitor the therapeutic effect. The Al^{18}F-DX600-BCH was obtained manually with a 20.4% ± 5.2% radiochemical yield without attenuation correction and an over 99% purified radiochemical purity, being stable *in vitro* within 4 hours and cleared rapidly in blood (the half-lives of the distribution phase and clearance phase were 2.12 min and 25.31 min, respectively). Results of both biodistribution and PET imaging showed that Al^{18}F-DX600-BCH was highly accumulated in the kidney ($SUV_{kidney/normal}$ > 50), and specific uptake in testis ($SUV_{testis/normal}$ > 10) was observed in rat images. The kidney (++), gastrointestinal (++) and bronchial (+++) cells were evidenced of ACE2 positive by IHC staining of rats. A total of 10 volunteers were enrolled and received PET/CT 1 hour and 2 hours after injection or dynamic PET/CT during 0-330 seconds (NCT04542863), from which strong radioactivity accumulation was mostly observed in the genitourinary system ($SUV_{renal\ cortex}$ = 32.00, SUV_{testis} = 4.56), and moderate accumulation in conjunctiva and nasal mucosa for several cases. This work firstly reported the probe Al^{18}F-DX600-BCH targeting ACE2, conducting preliminary preclinical experiments and a total of 10 clinical transformations, which demonstrated the potential and possibility of non-invasive mapping of ACE2. Trial registration: ClinicalTrials.gov NCT04542863. Registered 9 September 2020.

Introduction

Sweeping the world from the end of 2019 to the beginning of 2020, the Corona Virus Disease 2019 (COVID-19) has regularly become the focus of society and academia [1–4]. To date, according to statistics, the number of infections worldwide has exceeded 250 million, and the number of deaths has reached 5.1 million [5]. Faced with such a severe situation, there are more and more studies on the SARS-CoV-2 virus that caused the pandemic. Recent and early studies have shown that the combination of human angiotensin-converting enzyme (ACE2) and the virus spike protein (S protein) plays a decisive role in the process of virus invading cells[6–8].

Since the combined with ACE2 must be needed for SARS-CoV-2 to enter the cell, the understanding of the binding process and the study of the characteristics of human ACE2 have become the top priority. Research by Daniel et al. showed that the S protein of SARS-CoV-2 is similar to the S protein of SARS-CoV, and the similarity of the amino acid sequence between the two is 76% [9]. The S protein form of SARS-CoV-2 is a trimer, each monomer has about 1300 amino acids, of which more than 300 amino acids constitute the RBD (receptor binding domain) of the S1 subunit, and the S1 subunit The base binds to ACE2 on the surface of the recipient cell, and the S2 subunit then fuses the virus with the cell membrane. On March 27, 2020, Zhou et al. published the full-length structure of the new coronavirus receptor ACE2 analyzed by cryo-electron microscopy [10]. The S protein of SARS-CoV-2 binding to the peptidase domain (peptidase domain) of ACE2, ACE2 is successfully "kidnapped" by SARS-CoV-2, and can only "obediently"

open the channel allowing virus to enter the cell. The analysis of the full-length structure of ACE2 provides important structural biological support for the subsequent development of vaccines and antiviral drugs.

In order to detect the expression and distribution of ACE2 in humans in real time, especially in the process of viral infection, researchers have gradually begun the search and development of ACE2 inhibitors. In 2003, Huang et al. reported the ACE2 peptide inhibitor DX600 found by screening a restricted peptide library obtained from phage [11]. DX600 is a peptide with high affinity and selectively acting on ACE2 (Ki = 2.8 nmol), and it has no activity on homologous ACE. It is suitable for the construction of micro-dose nuclear medicine molecular imaging probes. In 2013, Liao et al. published an enzymatic method for recombinant and endogenous ACE2 neutralizing antibodies [12]. The crossover experiment of ACE and ACE2 further proves the specific detection ability of ACE2 inhibitor DX600. Western blotting and cell lysis experiments showed that DX600 has a significant inhibitory effect on ACE2 on the cell surface. Recently, a NOTA-conjugated DX600 peptides named ^{68}Ga-NOTA-PEP4 which was newly synthesized by Parker et al. showed specific binding in the heart, liver, lungs and intestine in the *in vivo* studies in a transgenic hACE2 murine model [13]. Our group also reported the constructions and the first clinical transformation of the novel ACE2 targeting probe named ^{68}Ga/^{64}Cu-HZ20 in the same period, which will help clarify the function of ACE2 *in vivo* and lay the experimental foundation for the development of ACE2-specific PET probes [14].

In this research, we obtained Al^{18}F-DX600-BCH with high affinity for ACE2, and for the first time carried out PET research to understand the expression of ACE2 in tissues and organs of volunteers and obtain the distribution of ACE2 in main organs. In addition, existing studies have shown that ACE2 is highly expressed in the malignant proliferation of colorectal cancer, kidney tumors, gastric cancer, pancreatic cancer and other tumors. The use of Al^{18}F-DX600-BCH PET imaging is expected to detect the ACE2 expression in healthy volunteers in real time, specifically and non-invasively, to study the distribution and expression of ACE2 receptors in the body, and to achieve therapeutic efficacy monitoring.

Materials And Methods

General

All chemicals, reagents, and solvents were purchased commercially without further purification. Sep-Pak Accell Plus QMA and Sep-Pak C18-Light cartridges were purchased from Waters, and an Acrodisc 25-mm syringe filter (0.2 mm) was purchased from Pall Corp. The no-carrier-added Na^{18}F was obtained from the Department of Nuclear Medicine, Peking University Cancer Hospital. DX600 and NOTA-DX600 were custom synthesized by ChinaPeptides Co., Ltd (Shanghai, China). The product was analyzed by radio–high-performance liquid chromatography (HPLC) (1200; Agilent) equipped with a g-detector (Bioscan) with mobile phases of H_2O (A) and acetonitrile (B) mixed with 0.1% trifluoracetic acid. Radio-HPLC was performed using a flexible A–B gradient (20% B in 0-5 min, 20-80% B in 5-10 min, 80% B in 10-12 min, 80-20% B in 12-15 min) with a flow of 1 mL/min and 220-nm ultraviolet light. Micro-PET/CT was performed

on the Mira® PET/CT of PINGSENG Healthcare Inc. (Shanghai, China). PET/CT scans were obtained on a Gemini TF scanner (Philips Medical Systems) with unenhanced low-dose CT. Al^{18}F-DX600-BCH PET/MRI was performed on a hybrid 3.0T PET/MR scanner (uPMR790, UIH, Shanghai, China) in female volunteers.

Radiolabeling and quality control

As shown in **Figure 1A**, radio-synthesis was based on a previous procedure [15]. $^{18}F^-$ was loaded onto a QMA cartridge and eluted by 0.5 mL of saline. No-carrier-added $^{18}F^-$ in saline (100 μL, 370-740 MBq), potassium hydrogen phthalate (KHP) buffer (11 μL, 0.5 M, pH 4.0), and $AlCl_3$ (6 μL, 2 mM) in KHP buffer (0.05 M, pH 4.0) were mixed and kept at room temperature for 5 min. Then, 10 μL of NOTA-DX600 (2 mM, 20 nmol) were added and the mixture was heated at 110 ℃ for 15 min. After cooling to room temperature, the reaction was diluted with 5 mL of H_2O and passed through a Sep-Pak C18-Light cartridge, which was pretreated with 5 mL of EtOH followed by 10 mL of H_2O. The Sep-Pak C18-Light cartridge was washed with H_2O (10 mL) and eluted with 0.6 mL of 80% EtOH to obtain the product, which was passed through a sterile filter membrane (0.22 mm) and diluted with saline for further studies. The radiochemical purity of Al^{18}F -DX600-BCH was analyzed by radio-HPLC. In vitro stability was studied by analyzing the radiochemical purity of Al^{18}F- DX600-BCH by incubating in saline for 4 h.

Pharmacokinetics, bio-distribution and micro-PET/CT

Blood samples of normal mice (KM mice) were collected to determine the ^{18}F-radioactivity in the whole blood. Each blood sample for ^{18}F radioactivity analysis was collected from the orbit and analyzed using an automatic gamma counter (Wizard, Wallac, Turku, Finland). Blood samples (0.1-0.2 mL) were collected at 1, 3, 5, 10, 15, 30, 45, 60, 120, 180 and 240 min after injection.Five male or female normal mice in each group were injected with 200 μL of Al^{18}F-DX600-BCH (0.74 MBq) via the tail vein. After 5, 30, 60, 120 and 240 min, the mice were sacrificed, and the blood, heart, liver, kidney, lung, spleen, stomach, small intestine, large intestine, muscle, bone, brain, and testis (for male mice) were collected, weighed, and measured for radioactivity by the g-counter. As a marker, 10 samples of 1% injected dose were taken from the injection and measured. The results are expressed as the percentage injected dose per gram (%ID/g). Normal mice and rats were intravenously injected with 200 μL of Al^{18}F-DX600-BCH (7.4 MBq, 3.7 GBq/μmol) vail the tail vein. The mice were anesthetized with 3% (v/v) isoflurane and underwent small-animal PET scans with continuous 1.5% (v/v) isoflurane. The images were obtained at 30, 90 and 180 min after injection.

Imaging was performed on a PINGSENG Mira® PET/CT scanner, and the images were displayed by Avator workstation software. The SUVmax value for regions of interest over testis, kidney, and muscle were measured.

PET/CT/MRI imaging and analysis

The Al^{18}F-DX600-BCH PET/CT imaging study was approved by the Ethics Committee of Beijing Cancer Hospital (approval 2020KT102), and registered in Chinese Clinical Trial Registry (ChiCTR2000037886, Date of registration: September 3, 2020) and ClinicalTrials.gov (NCT04542863, Date of registration: September 9, 2020) and all subjects signed an informed consent form. Considering the sink effect [16], 10 healthy volunteers were included (age, 50.5 ± 16.5 y; range, 34-67 y) (**Table 1**). Volunteers were intravenously injected with Al^{18}F-DX600-BCH (1.2–2.9 MBq/kg, 23-27 GBq/μmol) and underwent PET/CT or PET/MR at 1 and 2 h after injection or dynamic PET/CT during 0-330 s. Imaging was performed on a Gemini TF scanner (Philips Medical Systems) from head to middle of thigh. CT was performed using a voltage of 120 keV, a current of 100 mAs, a pitch of 0.8 mm, a single-turn tube rotation time of 0.5 s, and a scanning layer thickness of 3 mm. CT reconstruction used a standard method with a 512 × 512 matrix and a layer thickness of 3–5 mm. The PET images were acquired using a 3-dimensional model at 9–10 bed positions (90 s per bed position) and were reconstructed using ordered-subsets expectation maximization. Data from CT or MR imaging were used to correct the PET images for attenuation. Whole-body CT and PET images were eventually obtained. The SUVmax in regions of interesting were determined by 2 experienced physicians, and data such as SUVmean, average activity concentration (Bq/mm^3), and the volume of each organ at 1 and 2 h after injection were obtained to determine the organ biodistribution and to calculate the human organ dosimetry. Time-integrated activity coefficients were calculated individually [17], and human organ dosimetry was estimated using the OLINDA/EXM software (version 2.0; Hermes Medical Solutions AB) assuming no voiding of the urinary bladder until 2 h after injection as reported in the literature [18].

Immunohistochemistry

Harvested rats' tissues after imaging were formalin-fixed, paraffin-embedded, and sliced at 4 μm thickness. Endogenous peroxidase was blocked with 3% dioxygen at RT for 10 min. Antigen was retrieved from the tissue in citric acid buffer (pH 6.0) with microwave heating for 10min, followed cooled to room temperature. Tissues were blocked with goat antiserum for 30 min, incubated with rabbit anti-ACE2 antibody (1:100 ab108252, Abcam) at 4 ˚C overnight. And then the sections were stained using Super sensitive polymer HRP IHC detection system (PV-6000, ZSGB-BIO) for 30 min at RT. Subsequently, the sections were developed with 3, 3'-diaminobenzidine tetrahydrochloride (DAB), Hematoxylin redyeing，2% hydrochloric acid alcohol separation, dehydrated in an alcohol gradient, and sealed in neutral mounting media, and scanned (Aperio Versa 200, Leica).

Statistics

The data are presented as the mean ± SD. Comparisons of Al^{18}F-DX600-BCH uptake among different time point using paired t-tests. The two-tailed, unpaired Student's t-test was used to compare the differences between groups. A P value of 0.05 or less was considered statistically significantly. Subsequently, these data were summarized using descriptive statistics. Statistical analysis was performed using SPSS 26.0 (IBM Corporation, Armonk, New York, USA), Excel software (Microsoft

Corporation, Redmond, Washington, USA) Origin2020b software (OriginLab Corporation, Northampton, Massachusetts, USA) or Prism 8.0 software (GraphPad Software, USA).

Results

Synthesis and radiolabeling of $Al^{18}F$-DX600-BCH

The purchased DX600 polypeptide and a 0.05M KHP (potassium hydrogen phthalate) solution of $Na^{18}F$ and $AlCl_3$ were incubated at 110 °C for 15 min to obtain $Al^{18}F$-DX600-BCH. The radiochemical yield without time-decay correction was 20.4% ± 5.2%, and the specific activity was calculated to be 3.7-18.5 GBq/μmol (n=15). The purified radiochemical purity was analyzed by radio-HPLC to exceed 99%, and its retention time was 10.4 minutes (**Figur 1B**). The injection was colorless and transparent, with the neutral pH (6.5±0.5). The quality control results are shown in **Table 2**.

Radio-pharmacokinetics and biodistributions of $Al^{18}F$-DX600-BCH

$Al^{18}F$-DX600-BCH was prepared and purified by HPLC, with an *in vitro* stability test in 4 hours (**Figure 1B**). The pharmacokinetic curve showed that the concentration of $Al^{18}F$-DX600-BCH in the blood drops rapidly (the half-life was 2.12 min in the distribution phase, and was 25.31 min in the clearance phase), which may indicate rapid target seeking and metabolism (**Figure 1C**).

As shown in **Figure 1D**, at 5 min post-injection, kidney showed the highest uptake of $Al^{18}F$-DX600-BCH (27.60 ± 3.76 %ID/g), followed by the uptake in blood (7.29 ± 1.20 %ID/g) and lung (6.19 ± 0.46 %ID/g) in a short time. The uptake was significantly reduced at 240 min in blood (0.07 ± 0.01 %ID/g, -99.0 %, $P < 0.001$) and lung (0.28 ± 0.06 %ID/g, -95.5 %, $P < 0.001$). However, the uptake in kidney went up (36.01 ± 6.10 %ID/g at 60 min) and down (19.88 ± 2.11 %ID/g at 240 min) around a high level by the time. The low uptake in non-target organs caused high–ACE2 positive organs such as kidney to be located with the kidney/blood ratio of 284 at 240 min.

Micro-PET/CT Imaging

As illustrated in **Figure 2A**, the result of micro-PET/CT images in normal mice is consistent with that of the biodistribution data. At 30, 90 and 180 min post-injection, the uptake of $Al^{18}F$-DX600-BCH cannot be observed everywhere except kidneys and bladder.

Similarly, in normal rats, $Al^{18}F$-DX600-BCH was highly accumulated in kidneys and bladder, as well as can be obviously seen in testis at each time point (**Figure 2B**). The SUVmax ratios of testis-to-muscle and kidney-to-muscle were 12.0 and 67.5 at 30 min post-injection, 15.5 and 64.8 at 90 min post-injection, 19.3 and 77.7 at 180 min post-injection, respectively.

Rat immunohistochemical findings indicated that ACE2 is moderately positive (++) in the kidney, stomach, small intestine, large intestine, and is generally positive (+) in alveolar cells, but negative in the

heart, liver, and spleen. It is worth noting that highly positive ACE2 expression was observed in bronchial cells (+++) and liver plate marginal cells (++). These results are in agreement with our preclinical experiments.

PET/CT Imaging and Analysis

During PET/CT imaging of 10 volunteers, no adverse, clinically detectable pharmacologic effect or significant change in vital signs was observed. As shown in **Figure 3**, certain organs in urogenital system including kidneys, testis (male), uterus (female), breast (female), penis (male) had intense radioactivity accumulation, with an SUVmax of 45.73 ± 14.67, 6.45 ± 2.67, 3.73 ± 1.01, 2.76 ± 0.52 and 2.39 ± 0.65, respectively. Besides, uptake in pancreas (3.32 ± 0.67), blood pool (2.42 ± 0.58), nose (2.42 ± 0.40), and gallbladder (2.30 ± 0.92) was relatively high too, which is up with the reported ACE2 distribution (http://www.proteinatlas.org/). And the dynamic ROIs changing during 330 s in superior vena cava and aorta of one of volunteers were also shown in **Figure 3A**.

As shown in Figure 4, the representative whole body PET of a two healthy volunteers and (#002) at 90 min after injection. For the #001, a 47-year-old male, the calculated SUVmax value showed the renal cortex (32.00) and testis (4.56) showed high accumulation (**Figure 4A-D**). Analysis in the #002, a 54-year-old female, showed the breast (2.07) had moderate accumulation, while the renal cortex (34.75) and the ovary (2.11) showed high accumulation (**Figure 4E-H**). The high uptake observed in the genitourinary system agree with our preclinical and clinical findings (**Figure 3**).

Interestingly, in certain cases, moderate radioactivity accumulation had been observed in the conjunctiva (**Figure 5A**) and the nasal mucosa (**Figure 5B**) via transverse CT, PET and fusion images. And the PET images showed that the gall bladder (**Figure 6A**) had moderate radioactivity accumulation, and the bilateral ovary (**Figure 6B**) had moderate accumulation. A delayed PET/MR (2 h after Al^{18}F-DX600-BCH injection) examination was conducted immediately following PET/CT imaging to locate the precise foci of ovarian. These findings are consistent with the results of another latest work on ACE2 of the research team.

The estimated effective dose of Al^{18}F-DX600-BCH to adult was 0.00158 mSv/MBq (**Table 3**), which was much lower than the whole-body effective dose of 0.020 mSv/MBq of ^{18}F-FDG reported by International Commission on Radiological Protection's (ICRP). Among all the parts covered by calculation, the radiation dose of the kidney occupies the first place without any suspense (0.0327 mGy/MBq), which is much higher than other top-ranked organs, such as the liver (0.00370 mGy/MBq) and the adrenal glands (0.00365 mGy/MBq) and spleen (0.00252 mGy/MBq) in turn.

Discussion And Conclusion

Nuclear medicine PET (Positron Emission Tomography) probe is a cutting-edge technology commonly used in tumor diagnosis and treatment. It has the characteristics of high sensitivity, deep tissue penetration, and quantitative analysis. The drug injection dose can be controlled below 30 micrograms,

which leads to a safe and reliable non-invasive imaging method. Developing a new specific PET molecular probe targeting ACE2 is expected to detect ACE2 expression in systemic lesions non-invasively, real-time and quantitatively, and to detect the heterogeneity of ACE2 expression in the same lesion and different lesions. Observing the changes of ACE2 expression in treatment process is used to screen patients during the treatment of solid tumors with high expression of ACE2, monitor therapeutic effects, early warn of drug resistance and/or recurrence and metastasis, and realize individualized treatment in targeted tumor therapy.

A high-affinity human ACE2-specific peptide DX600 was selected and modified as a PET imaging agent for the distribution of ACE2 expression level, which may be related to the susceptibility, severity and prognosis of SARS-CoV-2 infection. Preclinical studies of Al^{18}F-DX600-BCH have shown that it has ideal pharmacokinetic properties, rapid blood clearance, low background organ uptake and clearance mainly through the kidneys.

After safety and dosimetry assessments, Al^{18}F-DX600-BCH was used to conduct human clinical translational studies on 10 volunteers of different ages and genders. In order to fully characterize this molecular imaging tool, each volunteer was scanned at the same time, and certain individuals were randomly selected for dynamic scanning. The results showed that the pharmacokinetics of 10 volunteers were highly consistent, and the organs with high expression of ACE2 (such as kidney, gall bladder, male testis, female uterus, etc.) were reflected in the high SUVmax and signal retention within 2 hours of the test. The plateau period for expressing tissue and blood pool clearance signals provides a convenient static image 60 minutes after administration, which can be used to analyze ACE2 expression.

The PET imaging of ACE2 quantitatively provides real-time and comprehensive receptor distribution by using the SUVmax value taken by Al^{18}F-DX600-BCH, which is directly related to the expression level of ACE2, which will have the opportunity to provide new information related to SARS-CoV-2 infection and pathology information. Some of our results highlight the expression profile in the reproductive organs. Recent studies have reported testicular damage caused by SARS-Cov-2 infection [19], [20], and this trend can be observed in every male volunteer as shown in Figure 4. Similarly, consistent with the results in the HPA database (http://www.proteinatlas.org), in addition to the ACE2 expression observed in the breasts of young women, Al^{18}F-DX600-BCH uptake was observed in the ovaries of women of all ages.

It is worth noting that, the uptake of Al^{18}F-DX600-BCH in the lung and heart is low, but is high in the nasal mucosa. This may be related to the way the virus infects the respiratory tract [21]. Many clinical reports also indicate that partial or even complete loss of smell is an early symptom of SARS-CoV-2 infection [22], [23]. This observation is consistent with recent studies using high-sensitivity RNA in situ mapping, which showed that ACE2 expression is highest in the nose and decreases along the lower respiratory tract [24]. This trend is consistent with our clinical statistics.

Based on the safety considerations of radioactive probes in humans, we calculated Al^{18}F-DX600-BCH of relevant doses *in vivo*. The mean absorbed doses in the organs per unit of administered activity were

calculated by the OLINDA/EXM software for the given residence times determined from the measured Al^{18}F-DX600-BCH distribution in the body of female mice. The average effective dose per unit of drug delivery activity was 0.00158 mSv/MBq, which is lower than that of PET-scans with ^{18}F-FDG and below the drug administration limit recommended in the study (Table 3).

Reviewing this study, as a non-head-to-head comparison to our previous work of ^{68}Ga/^{64}Cu-HZ20, meaningful conclusions can be given [14]. And the high Al^{18}F-DX600-BCH uptake in testis of rats is also consistent with the finding in human in our reported cases. Additionally, as founded in clinical PET, ovarian and gallbladder exhibits the similar uptakes, and confirmed by PET/MR, due to the equipment's technology advantages. Furthermore, moderate radioactivity accumulation can be observed in conjunctiva and nasal mucosa in certain cases from both transverse CT, PET and fusion images, which is similar to results of the former work. As the most widely used nuclide in contemporary PET/CT, F-18 has a more moderate half-life than Ga-68 and Cu-64 with more stable and large-scale production, which allows F-18 labeled probes to have more application value in first-line diagnosis and treatment, and a better prospect in clinical transformation. Thus, it is reasonable to draw that Al^{18}F-DX600-BCH could be used as a drug targeting ACE2 for further clinical research, and it is hopeful to say that more clinical data can be obtained from clinical research to evaluate the distribution of ACE2 in healthy or diseased humans.

All in all, we have developed a non-invasive imaging method that uses Al^{18}F-DX600-BCH PET to map human ACE2 (the key receptor for SARS-CoV-2 infecting human cells). This study used F-18 as a radionuclide to verify the results of the ^{68}Ga/^{64}Cu-HZ20 probe published by our team for the first time. The results of 10 volunteers were consistent with the pathology report of the receptor distribution. These preliminary results require further investigation in a wider volunteer population. Due to the non-invasive quantitative detection of stable and transient ACE2 expression, this quantitative imaging method may be helpful in assessing differences in SARS-CoV-2 infectivity between individuals; the severity and duration of COVID-19 symptoms; and the evaluation of other novelties emergence and the physiological role of the new coronavirus.

This work reported on the new probe Al^{18}F-DX600-BCH targeting ACE2, and conducted preliminary animal experiments as well as a total of 8 clinical transformations. This research firstly shows the potential and possibility of meeting the needs of non-invasive ACE2 mapping.

Declarations

Funding

This work was supported by National Natural Science Foundation (82171973, 82171980, 81871386, 81871387), Beijing Municipal Administration of Hospitals-Yangfan Project (ZYLX201816), Beijing Excellent Talents Funding (2017000021223ZK33), Beijing Millions of Talent Projects A level funding (No. 2019A38).

Conflicts of interest

The authors declare that they have no conflict of interest.

Availability of data and material

The datasets used and/or analysed during the current study are available from the corresponding author on reasonable request.

Code availability

Not applicable.

Authors' contributions

H. Z., X. Y. and Z. Y. conceived and designed the experiments. J. D. and Q.Z. radio-synthesized and characterized the agent. J. D. and Q.Z. conducted preclinical research and quality control of radio-tracer. N. Z., J. J., and Z. L. performed the PET, PET/CT and PET/MRI studies. Z. W. performed the immunohistochemistry and dose calculations. F. W. conducted nuclide production. J. D., N. Z., J. J., X. M., and T. L. analyzed the data. J. D., N. Z., and H. Z. co-wrote the paper. J. D. and H. Z. provided constructive discussion. All authors discussed the results and analysis and commented on manuscript.

Ethical approval

All procedures performed in studies involving human participants, registered in ClinicalTrials.gov (NCT04542863, Date of registration: September 9, 2020), were in accordance with the ethical standards of the Ethics Committee of Peking University Cancer Hospital (2020KT102) and with the latest guidelines of the Declaration of Helsinki. The protocol approved by the Peking University Cancer Hospital Animal Care and Use Committee and the Department of Comparative Medicine at the Washington University in St. Louis School of Medicine (Protocol Number 20190006 and 20-0183) for the care and use of animals were followed.

Consent to participate

Not applicable.

Consent for publication

Not applicable.

References

1. Tan HW, Xu Y-M, Lau ATY. Angiotensin-converting enzyme 2: the old door for new severe acute respiratory syndrome coronavirus 2 infection. Rev Med Virol 2020; 30: e2122.

2. World Health Organization. Coronavirus disease 2019 (COVID-19): situation report, 49. 2020; https://www.who.int/emergencies/diseases/novel-coronavirus-2019/situation-reports.
3. Sheshe S, Nazifi A, Labbo AM, Khalid GM, Yahya A, Muhammad U, Haruna AM. Mechanism of Antiviral Immune Response and COVID-19 Infection. Asian J Immuno 2020; 3: 1-8.
4. Yang X, Yu Y, Xu J, et al.Clinical course and outcomes of critically ill patients with SARS-CoV-2 pneumonia in Wuhan, China: a single-centered, retrospective, observational study. Lancet Resp. Med. 8, 475-481 (2020).
5. COVID-19 dashboard by the Center for Systems Science and Engineering (CSSE) at Johns Hopkins University. https://coronavirus.jhu.edu/map.html (2021).
6. Wang M, Cao R, Zhang L, Yang X, Xiao G. Remdesivir and chloroquine effectively inhibit the recently emerged novel coronavirus (2019-nCoV) in vitro. Cell Res 2020; 30: 269-271.
7. Roy B. COVID-19 pandemic: How close are we for an effective therapy? J Biomed Sci 2020; 7: 1-3.
8. Li Y, Wei Z, Li Y, Ran Y. Physiological and pathological regulation of ACE2, the SARS-CoV-2 receptor. Pharmacol Res 2020; 157: 104833.
9. Wrapp D, Wang N, Corbett KS, et al. Cryo-EM structure of the 2019- nCoV spike in the prefusion conformation. Science 2020; 367(6483): 1260-1263.
10. Yan R, Zhang Y, Li Y, et al. Structural basis for the recognition of SARS-CoV-2 by full-length human ACE2. Science 2020; 367(6485): 1444-1448.
11. Huang LL, Sexton DJ, Skogerson K, et al. Novel Peptide Inhibitors of Angiotensin-converting Enzyme 2. J Biol Chem 2003; 278(18): 15532-15540.
12. Liao K, Sikkema D, Wang C, et al. Development of an enzymatic assay for the detection of neutralizing antibodies against therapeutic angiotensin-converting enzyme 2 (ACE2). J Immunol Methods 2013; 389(1-2): 52-60.
13. Parker M, Blecha J, Rosenberg O, et al. Cyclic gallium-68 labeled peptides for specific detection of human angiotensin-converting enzyme 2. J Nucl Med 2021; 62(9): 1-23
14. Zhu H, Zhang H, Zhou N, et al. Molecular PET/CT profiling of ACE2 expression in vivo: implications for infection and outcome from SARS-CoV-2. Adv Sci 2021; 8: 2100965.
15. D'Souza CA, McBride WJ, Sharkey RM, Todaro LJ, Goldenberg DM. Highyielding aqueous ^{18}F-labeling of peptides via Al^{18}F chelation. Bioconjug Chem 2011; 22: 1793-1803.
16. Filss C, Heinzel A, Müller B, Vogg ATJ, Langen KJ, Mottaghy FM. Relevant tumor sink effect in prostate cancer patients receiving ^{177}Lu-PSMA-617 radioligand therapy. Nucl Med 2018; 57: 19-25.
17. Cho SY, Gage KL, Mease RC, et al. Biodistribution, tumor detection, and radiation dosimetry of ^{18}F-DCFBC, a low-molecular-weight inhibitor of prostate-specific membrane antigen, in patients with metastatic prostate cancer. J Nucl Med 2012; 53: 1883-1891.
18. Green MA, Eitel JA, Fletcher J, et al. Estimation of radiation dosimetry for ^{68}Ga-HBED-CC (PSMA-11) in patients with suspected recurrence of prostate cancer. Nucl Med Biol 2017; 46: 32–35.

19. Yang M, Chen S, Huang B, et al. Pathological findings in the testes of COVID-19 patients: clinical implications. Eur Urol Focus 2020; 6(5): 1124-1129.
20. La Marca A, Busani S, Donno V, Guaraldi G, Ligabue G, Girardis M. Testicular pain as an unusual presentation of COVID-19: a brief review of SARS-CoV-2 and the testis. Reprod Biomed Online 2020; 41(5): 903-906.
21. Wang L, Wang Y, Ye D, Liu Q. Review of the 2019 novel coronavirus (SARS-CoV-2) based on current evidence. Int J Antimicrob Agents 2020; 55: 105948.
22. Lechien JR, Chiesa-Estomba CM, De Siati DR, et al. Olfactory and gustatory dysfunctions as a clinical presentation of mild-to-moderate forms of the coronavirus disease (COVID-19): a multicenter European study. Eur Arch Otorhinolaryngol 2020; 277: 2251-2261.
23. Moein ST, Hashemian SM, Mansourafshar B, Khorram-Tousi A, Tabarsi P, Doty RL. Smell dysfunction: a biomarker for COVID-19. Int Forum Allergy Rhinol 2020; 10: 944-950.
24. Hou YJ, Okuda K, Edwards CE, et al. SARS-CoV-2 reverse genetics reveals a variable infection gradient in the respiratory tract. Cell 2020; 182: 429-446.

Tables

Table 1 The demographic data of all volunteers.

Healthy Volunteers (V)	Age (year)	Sex	Weight (kg)	Injected Dose (MBq)
HV1	47	M	57	105.08
HV2	54	F	90	147.36
HV3	58	F	75	217.56
HV4	61	F	73	210.9
HV5	39	M	70	162.06
HV6	36	F	60	158.36
HV7	42	F	47	83.25
HV8	67	F	42	91.39
HV9	65	F	70	193.14
HV10	40	M	72	89.91

Table 2 The quality control (QC) of Al^{18}F-DX600-BCH.

Parameter	QC Specification	QC Result
Appearance	Clear, colourless	Pass
Volume	1.0-2.0 mL	1.5 mL
pH	5.0-8.0	7.4
Radio-TLC	> 95%	> 99%
Radio-HPLC	> 95%	> 99%
Ethanol	< 5%	1%
Endotoxins	< 15 EU/mL	<0.05 EU/ml
Sterility	Sterile	Pass
Specific Activity	13.5-100 GBq/μmol	25 GBq/μmol

Table 3 Estimated human organ radiation dosimetry of Al^{18}F-DX600-BCH by female model (mSv/MBq).

Target Organ	Beta (mGy/MBq)	Gamma (mGy/MBq)	Total (mGy/MBq)
Adrenals	3.78E-04	3.27E-03	3.65E-03
Brain	6.38E-04	6.65E-04	1.30E-03
Breasts	2.25E-04	4.48E-04	6.73E-04
Esophagus	2.26E-04	9.33E-04	1.16E-03
Eyes	2.25E-04	4.93E-04	7.19E-04
Gallbladder Wall	2.26E-04	2.11E-03	2.34E-03
Left colon	2.25E-04	1.10E-03	1.32E-03
Small Intestine	6.88E-04	1.09E-03	1.78E-03
Stomach Wall	2.72E-04	1.06E-03	1.33E-03
Right colon	2.29E-04	1.07E-03	1.30E-03
Rectum	4.40E-04	6.80E-04	1.12E-03
Heart Wall	4.66E-04	9.20E-04	1.39E-03
Kidneys	2.45E-02	8.26E-03	3.27E-02
Liver	1.62E-03	2.08E-03	3.70E-03
Lungs	1.43E-03	9.26E-04	2.36E-03
Ovaries	2.25E-04	7.37E-04	9.62E-04
Pancreas	2.30E-04	1.60E-03	1.83E-03
Salivary Glands	2.25E-04	5.01E-04	7.26E-04
Red Marrow	1.60E-04	9.19E-04	1.08E-03
Osteogenic Cells	1.43E-03	8.59E-04	2.29E-03
Spleen	3.96E-04	2.12E-03	2.52E-03
Thymus	2.41E-04	7.27E-04	9.68E-04
Thyroid	2.25E-04	5.75E-04	8.00E-04
Urinary Bladder Wall	2.25E-04	4.83E-04	7.08E-04
Uterus	2.25E-04	7.03E-04	9.28E-04
Total Body	4.83E-04	7.36E-04	1.22E-03
Effective Dose			1.58E-03 (mSv/MBq)

.

Figures

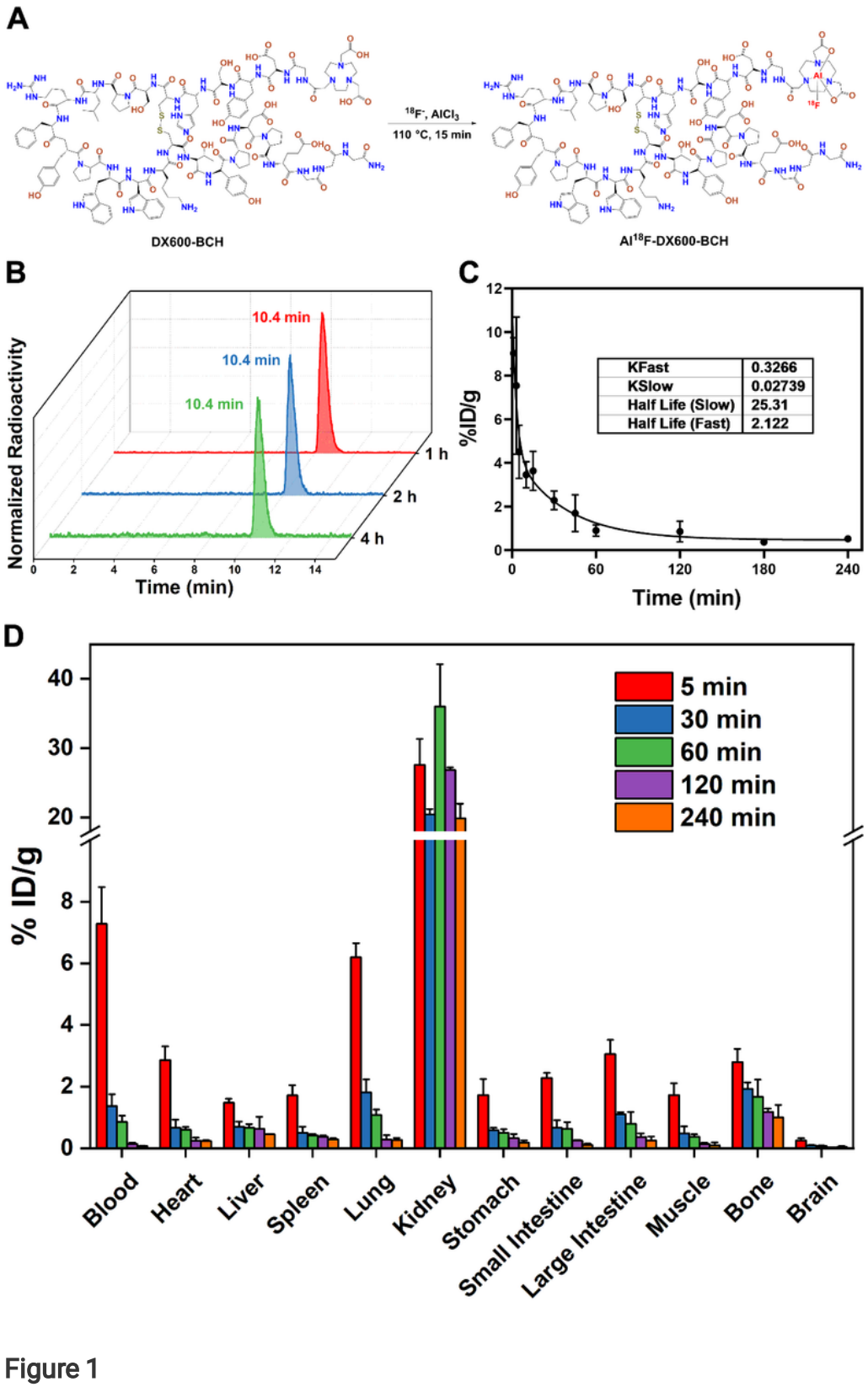

Figure 1

The preclinical experiment of Al18F-DX600-BCH. (A) Ligand structure and schematic diagram of radiolabel. (B) Stability analysis of Al18F-DX600-BCH over time in 0.01 M PBS solution at 37°C. (C) The

pharmacokinetic curve of Al18F-DX600-BCH in the blood of normal KM mice. (D) The bio-distribution of Al18F-DX600-BCH in female KM mice (n = 4).

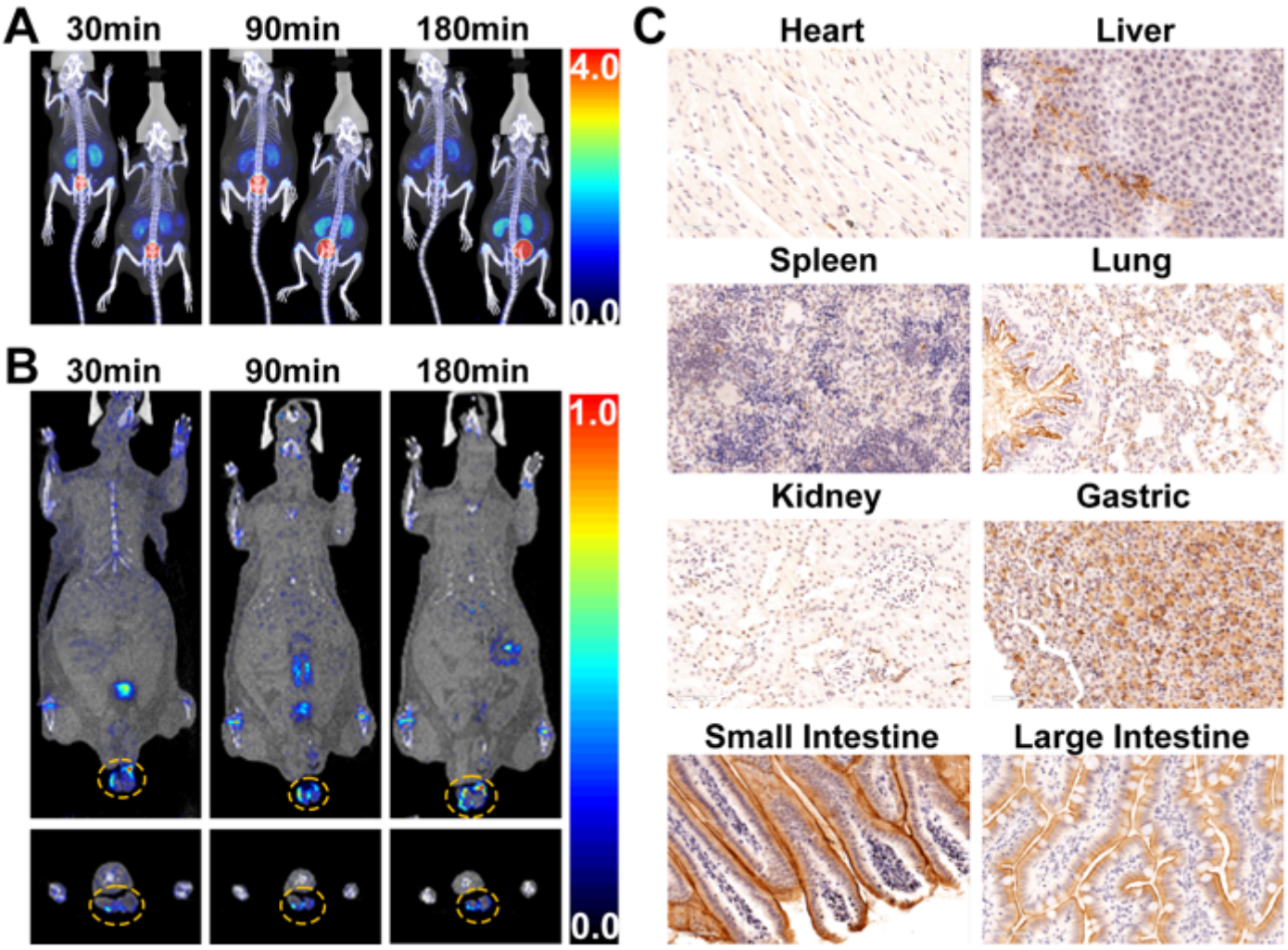

Figure 2

Micro-PET/CT imaging of Al18F-DX600-BCH in normal mice and rats at 30, 90, 180 min post-injection. (A) MIP images of two mice. (B) coronal diagrams and cross-sectional images of a rat. The testis of rat is marked with a yellow dotted circle. (C) Immunohistochemistry results of representative rats tissue.

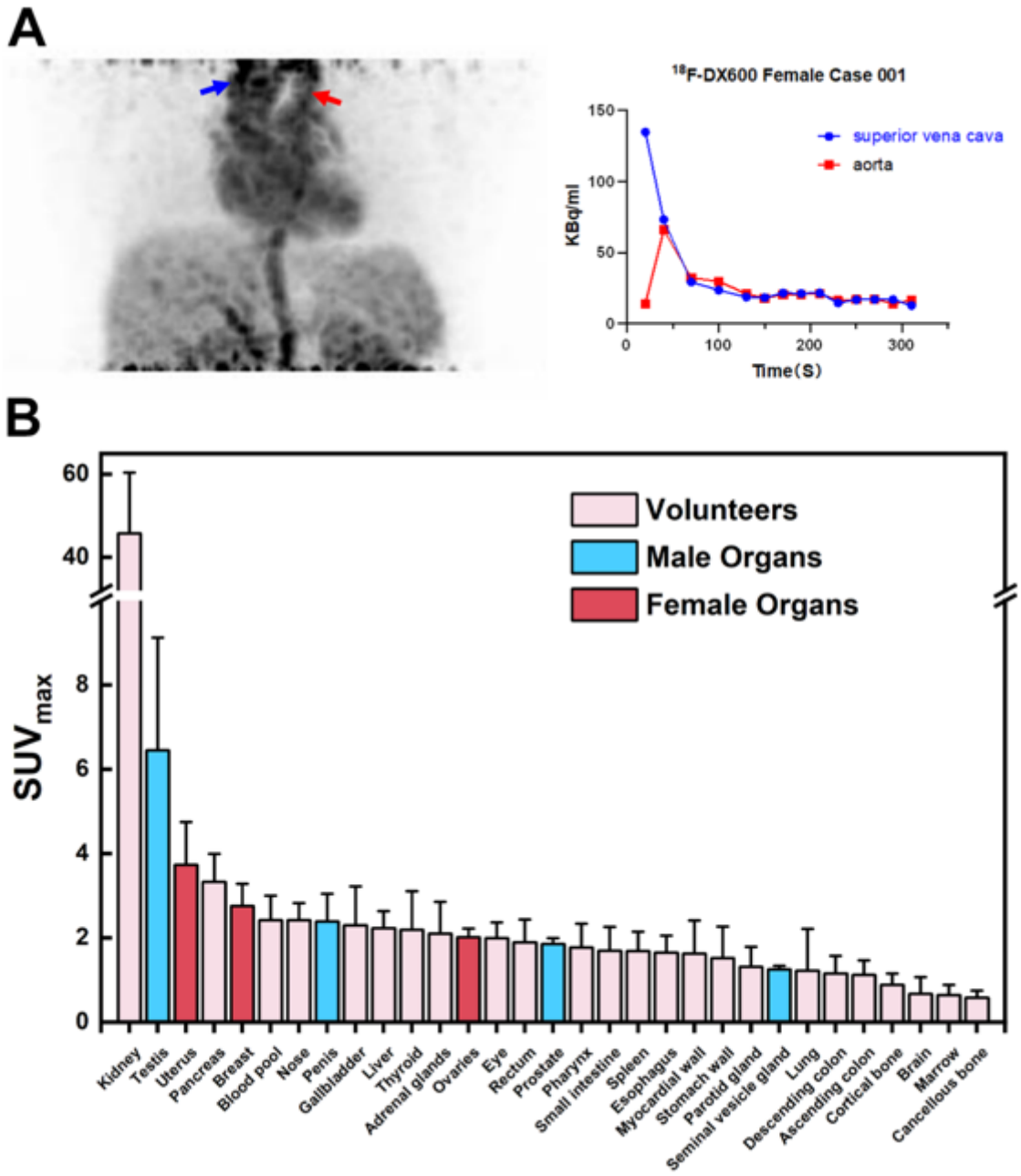

Figure 3

Al18F-DX600-BCH distribution in volunteers. (A) The dynamic changes of the uptake (kBq/mL) of superior vena cava and aorta at 13 time points (20, 40, 70, 100, 130, 150, 170, 190, 210, 230, 250, 290, 330 s) were listed. (B) Rank ordering of organ ACE2 expression in different organs indicated by SUVmax. The average SUVmax from 10 healthy volunteers at 60 min scans were shown in the column (blue: only for male, red: only for female).

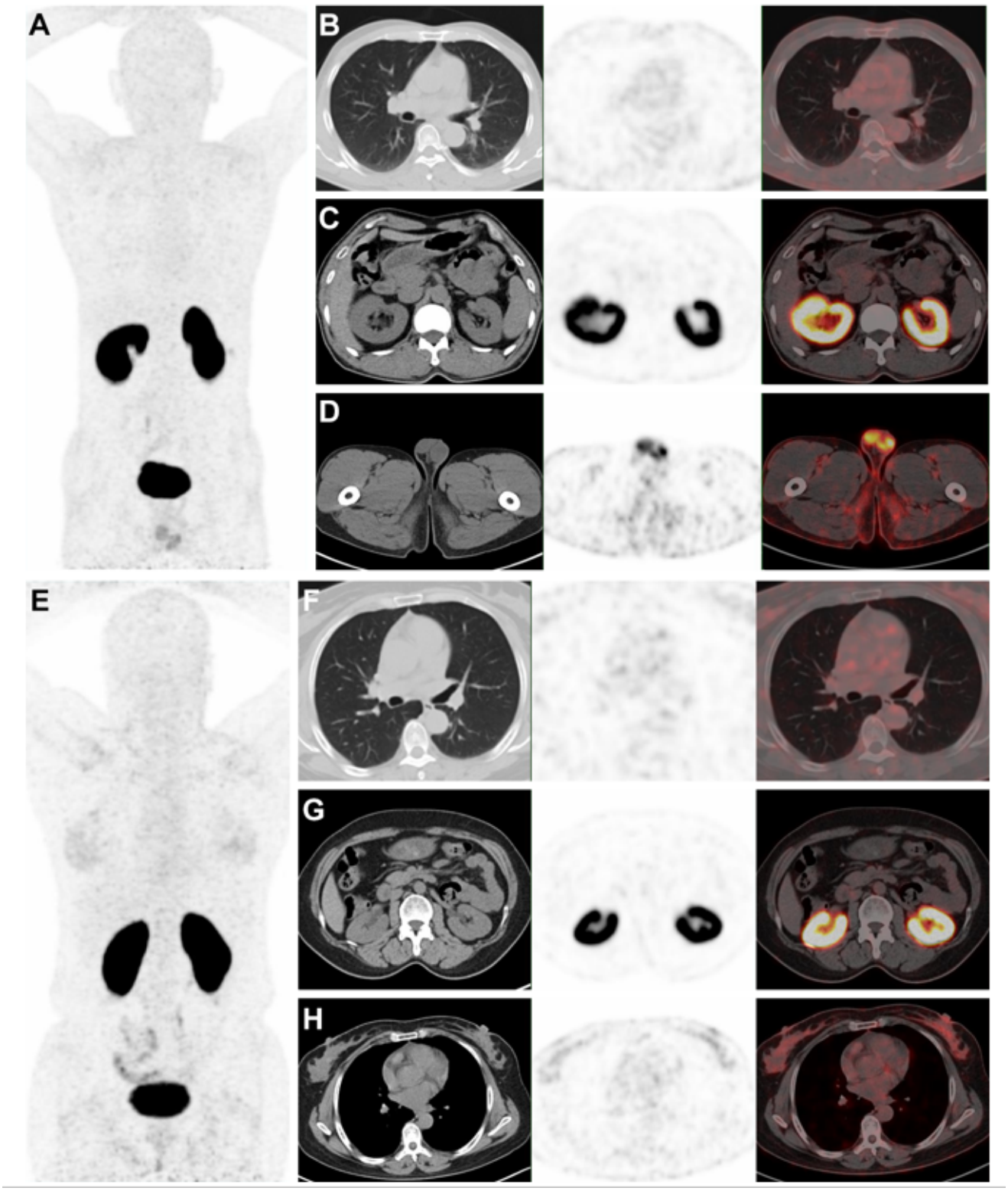

Figure 4

Typical PET imaging of Al18F-DX600-BCH in a 47-year-old male volunteer (HV1) and a 54-year-old female volunteer (HV2) at 90 min post-injection. The MIP (A) and transverse image showed that the lung (B) had mild radioactivity accumulation, the renal cortex (C) and testis (D) had high accumulation. The MIP (E) and transverse CT, PET and fusion images showed that the lung (F) had mild radioactivity accumulation, the renal cortex (G) had high accumulation, and the breast (H) had moderate accumulation.

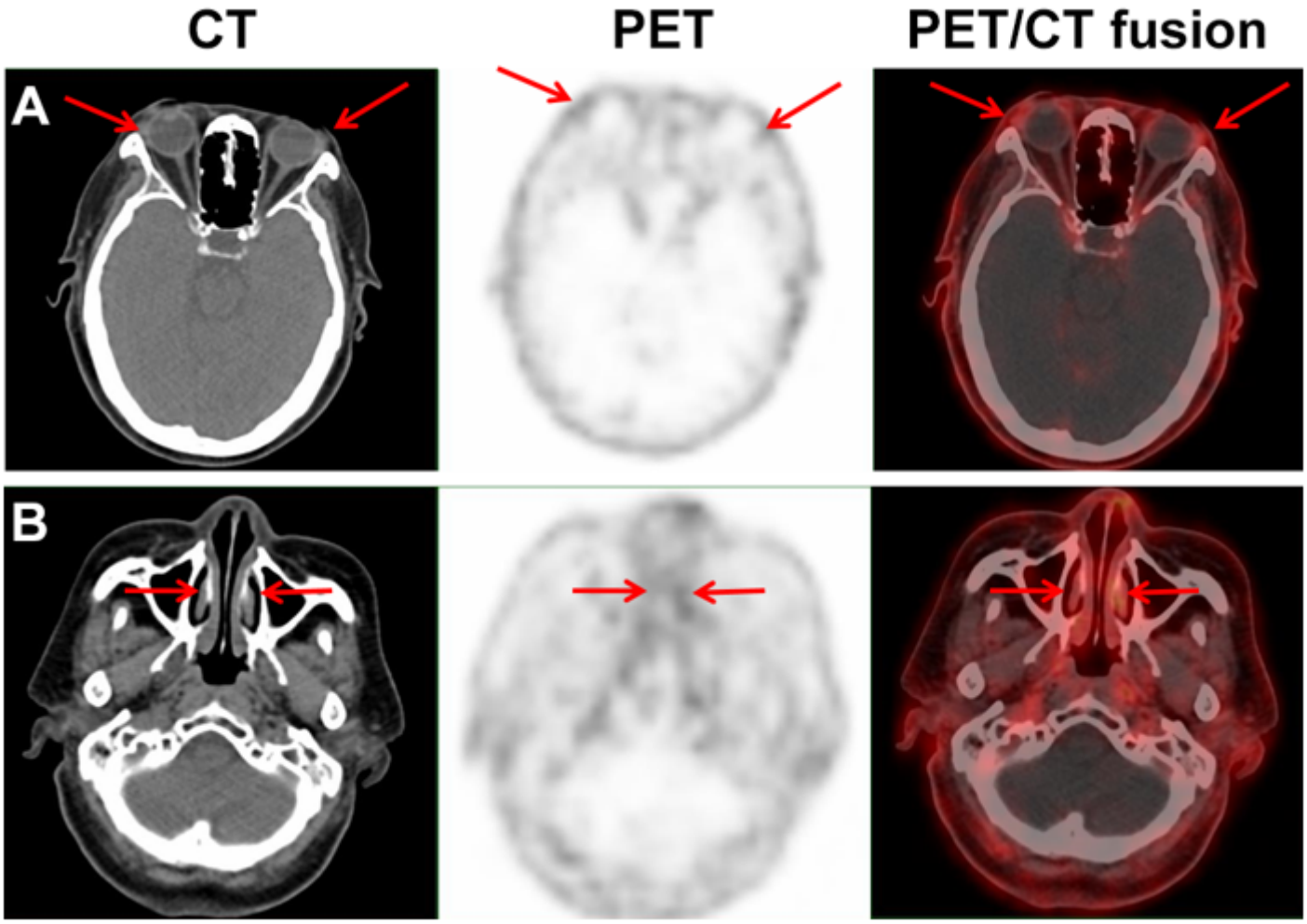

Figure 5

PET imaging of Al18F-DX600-BCH in volunteer (HV9). The transverse CT□PET and fusion images showed that the conjunctiva (A) and the nasal mucosa (B) had moderate radioactivity accumulation.

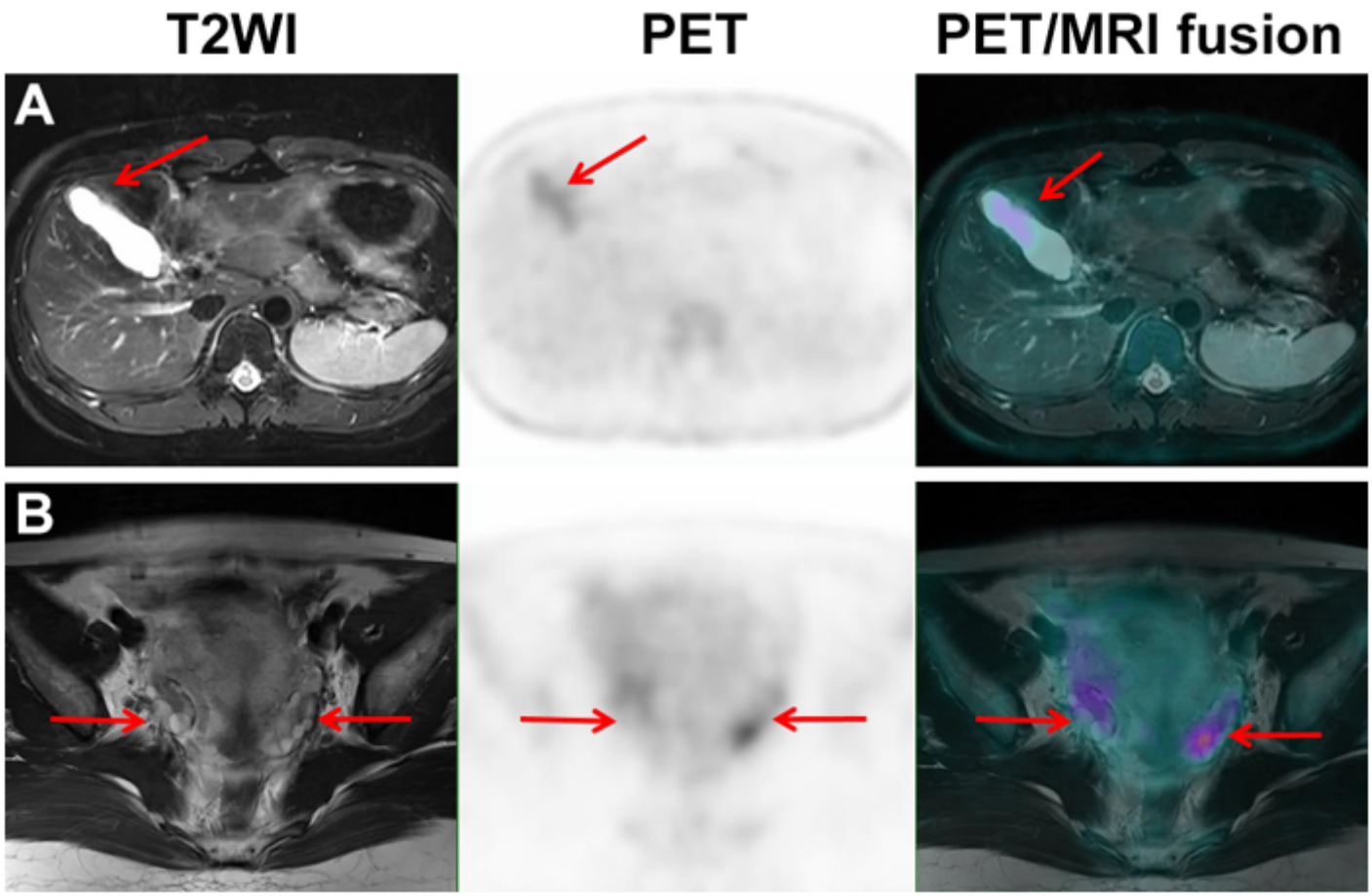

Figure 6

Al18F-DX600-BCH uptake observed in gallbladder and ovary, and confirmed with PET/MR. PET/MRI imaging of 18F-DX600 in a 36-year-old female volunteer (HV6). The transverse T2WI□PET and fusion images showed that the gall bladder (A) had moderate radioactivity accumulation , and the bilateral ovary (B) had moderate accumulation. PET/MR examinations were carried out at 2 h post-injection of Al18F-DX600-BCH on the same day.